JACS
JOURNAL OF THE AMERICAN CHEMICAL SOCIETY
Article
pubs.acs.org/JACS

Manipulating Magnetism at Organic/Ferromagnetic Interfaces by Molecule-Induced Surface Reconstruction

Rui Pang,[†,‡] Xingqiang Shi,[*,†] and Michel A. Van Hove[¶]

[†]Department of Physics, South University of Science and Technology of China, Shenzhen 518055, China
[‡]School of Physics and Engineering, Zhengzhou University, Henan 450001, China
[¶]Institute of Computational and Theoretical Studies and Department of Physics, Hong Kong Baptist University, Hong Kong, China

Supporting Information

ABSTRACT: Fullerenes have several advantages as potential materials for organic spintronics. Through a theoretical first-principles study, we report that fullerene C_{60} adsorption can induce a magnetic reconstruction in a Ni(111) surface and expose the merits of the reconstructed C_{60}/Ni(111) *spinterface* for molecular spintronics applications. Surface reconstruction drastically modifies the magnetic properties at both sides of the C_{60}/Ni interface. Three outstanding properties of the reconstructed structure are revealed, which originate from reconstruction enhanced spin-split π–d coupling between C_{60} and Ni(111): (1) the C_{60} spin polarization and conductance around the Fermi level are enhanced simultaneously, which can be important for read-head sensor miniaturization; (2) localized spin-polarized states appear in C_{60} with a spin-filter functionality; and (3) magnetocrystalline anisotropic energy and exchange coupling in the outermost Ni layer are reduced enormously. Surface reconstruction can be realized simply by controlling the annealing temperature in experiments.

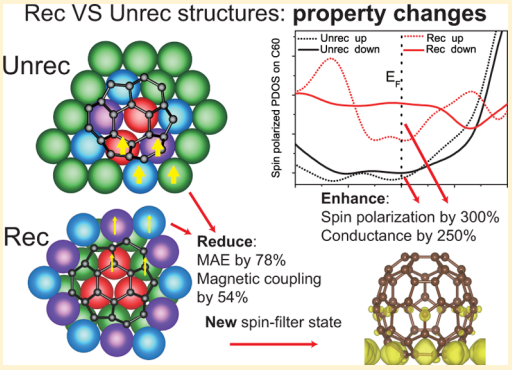

INTRODUCTION

Nonmagnetic/ferromagnetic interfaces of magnetic hard disk drives are crucial for their performance. To achieve read-head sensor miniaturization, it is essential to minimize the resistance of the system to maintain an ideal data-transfer rate and signal-to-noise ratio; at the same time, a large magnetoresistance (MR) ratio is decisive for optimum functionality of read-heads.[1,2] It is therefore desired to find a method that can simultaneously increase the MR ratio and the conductance of the device.[3] Recently, tuning the properties at organic/ferromagnetic interfaces by aromatic molecules has attracted broad attention.[4−6] Due to the π–d hybridization, chemical adsorption of aromatic molecules on magnetic surfaces produces new spin-split hybridized states at the interface (called a *spinterface*).[7−14] These states can be used to produce thermally robust molecular spintronic devices.[15] A challenge of this method is that chemical adsorption usually broadens the molecular orbitals near the metal Fermi level, which acts against the desired appearance of spin-polarized and energy-concentrated states.[15,16] Another possible use of the organic/ferromagnetic interface is modification of the magnetic interaction of surface atoms by the adsorbate.[14,17−20] Thus, it is possible to create hard/soft composite magnetic structures by self-assembly in molecular adsorption to achieve desired applications in permanent magnets, recording media and spintronics.[21]

Fullerenes and their derivatives are building blocks of potential high-performance organic devices.[22−27] Meanwhile, it has been proven that C_{60} adsorption can induce *nonmagnetic* metal surface reconstruction, i.e., rearrangement with different bonding of surface atoms,[28−33] just like other molecules which can provide strong interaction to the substrate.[34,35] These reconstructions have decisive influences on the their charge transport properties.[36] Thus, extending to *magnetic* metal surfaces, one can expect that adsorption-induced reconstruction could also have significant effects on the spin transport properties of fullerene/ferromagnetic interfaces. It is crucial to identify the existence and magnetic effects of reconstruction at these organic/ferromagnetic interfaces. As a magnetic metal, Ni can serve as a good substrate material to form a model system with C_{60}. The lattice mismatch of C_{60} on Ni(111) is only 0.3%. The commensurate 4 × 4 lattice was identified by low-energy electron diffraction (LEED) experiments.[37,38] More importantly, height profile measurements with scanning tunneling microscopy (STM) show that C_{60} can adsorb at different heights above the Ni(111) surface,[39] which is a hint for surface reconstruction. However, the reconstructed atomic structure and the effects of reconstruction on interface magnetic properties have not been studied to our knowledge.

In this paper, we investigate the geometric and magnetic properties of the C_{60}/Ni(111) interface by first-principles methods. We show that the reconstructed structure is energetically favored over the unreconstructed one. We

Received: October 20, 2015
Published: March 11, 2016

DOI: 10.1021/jacs.5b10967
J. Am. Chem. Soc. 2016, 138, 4029−4035

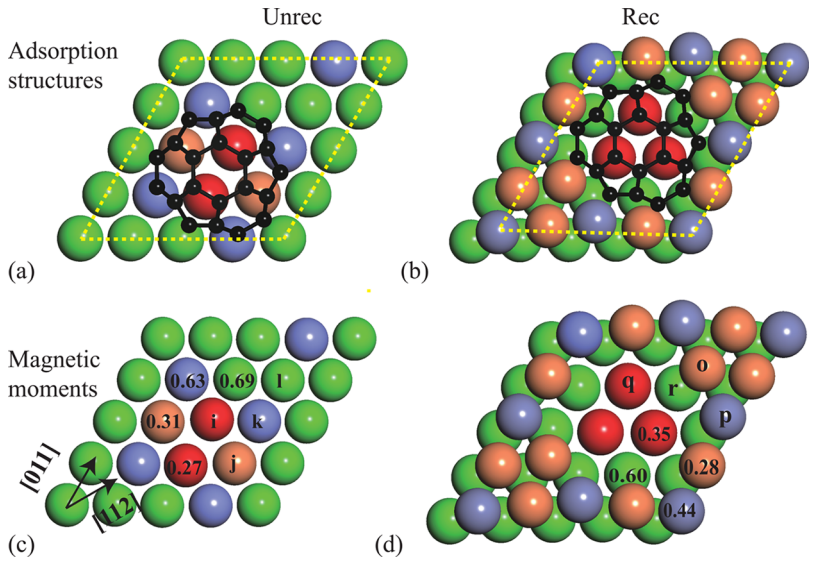

Figure 1. (a and b) Top views of the unreconstructed (Unrec) and reconstructed (Rec) structures of C_{60}/Ni(111); only the bottom part of C_{60} and the top layer(s) of Ni are shown; the dashed lines outline a Ni(111)-(4 × 4) surface unit cell. Different types of surface atoms are labeled with different colors classified by their magnetic moments and their distances from the C_{60} carbon atoms. (c and d) Magnetic moments (in μ_B) of surface atoms in Unrec and Rec structures; the molecule is removed for clarity.

demonstrate that, in comparison with the unreconstructed structure, the reconstructed one has the following superior properties: (1) the density of states (DOS) and the spin polarization of C_{60} are enhanced simultaneously around the Fermi level; (2) the molecular spin-polarized states are concentrated in energy around the Fermi level; (3) the magnetic coupling and magnetocrystalline anisotropic energies (MAE) of atoms in the outermost substrate layer are significantly reduced. The above changes in properties show that one can significantly affect magnetism at the organic/ferromagnetic interface through surface reconstruction. This prediction could have further applications in molecular and organic spintronics, and other areas related to magnetism of organic/ferromagnetic system.

METHODS

Calculations were performed using the plane-wave-basis-set Vienna ab initio simulation package (VASP).[40] The Ni(111) surface was modeled by a five-layer-slab with a 4 × 4 surface unit cell per C_{60}, which cell size is determined from low-energy electron diffraction experiments.[37,38] The convergence of the substrate thickness was further checked by a calculation with a 9-layer-slab with dipole correction along the vertical direction, showing that a five-layer-slab gives enough accuracy around the Fermi level. Projector augmented wave potentials[41] were employed with a kinetic energy cutoff of 500 eV and with a *K*-point sampling of 4 × 4. For the exchange-correlation functional, the Perdew-Burke-Ernzerh of generalized gradient approximation was utilized.[42] The calculations of magnetic couplings and MAE utilized the Quantum Espresso package[43] with equivalent computational parameters as in the VASP calculations. The adsorption structures with and without reconstruction were selected by (a) symmetry and size-matching between C_{60} and the Ni(111) surface, and (b) the informations of the same and similar systems[29−32,39,44,45] (for details see the Supporting Information).

RESULTS AND DISCUSSION

Figure 1 shows the most stable structures for both the reconstructed and unreconstructed cases (Rec and Unrec, respectively). Their stabilities, i.e., adsorption energies corrected for vacancy formation energies, are −2.13 eV for Unrec and −3.41 eV for Rec (see Supporting Information). Hence, the reconstructed structure is more stable.

As shown in Figure 1a,b, C_{60} binds with Ni through a C_6 hexagon parallel to the Ni(111) surface. In Unrec, the center of C_{60} is located above a bridge site of the surface. Six C−Ni bonds are formed with bond lengths ranging from 2.0 to 2.05 Å. In Rec with a 7-atom-cavity (Figure 1b), the molecule is located at an fcc-hollow site of the second Ni layer. Three C atoms of the lowest C_6 hexagon bind to three Ni ("q" in Figure 1d) in the second layer, while six C in the next-higher layer of C_{60} bind to six Ni ("o") atoms in the top surface layer, forming nine C−Ni bonds in all. The corresponding bond lengths range from 1.93 to 2.00 Å, indicating stronger bonding strength than with the unreconstructed substrate. The formation of more and stronger C−Ni bonds in Rec surpasses the energy cost of forming a seven-atom hole in the surface, making the Rec structure more stable. The C_{60}/Ni(111) system was investigated previously by STM,[39] and two adsorption configurations were found. C_{60} in one configuration was found to be 2.2 Å lower than the other, based on the measured apparent height profile.[39] The C_{60} height difference between Rec and Unrec in our calculation is 2.0 Å, by defining the molecular height as the height of the outermost C_{60} hexagon above the average height of the second substrate layer's Ni atoms. Thus, the low and high configurations in the STM experiment can be interpreted to be the Rec and Unrec structures in our calculation. The coincidence in molecular height between theory and experiment supports the reliability of our proposed structures, with further support from the existence of similar missing-atom structures of C_{60} on Cu, Ag, Au, and Pt(111).[29−33]

We quantify the spin-dependent charge transfer by the Bader charge analysis method.[46] In Unrec, 0.64 electrons are donated into each C_{60} from the metal substrate, among which 0.26 electrons occupy spin-up states while the other 0.38 occupy spin-down states. The charge transfer increases to 1.82 electrons in Rec, of which 0.85 are spin-up electrons and 0.97 are spin-down electrons. These charge transfers have significant effects on the electronic and magnetic properties of both the adsorbed C_{60} and the Ni surface, as detailed below.

DOI: 10.1021/jacs.5b10967
J. Am. Chem. Soc. 2016, 138, 4029−4035

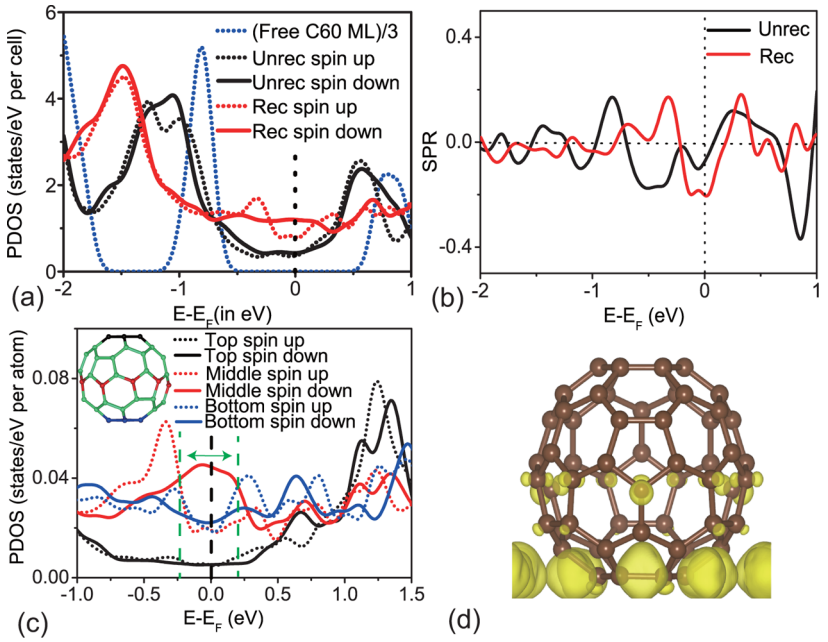

Figure 2. (a) PDOS of free C_{60} monolayer, and of C_{60} in Rec and Unrec structures. (b) Spin-polarization ratio (SPR) of C_{60} in Rec and Unrec. (c) PDOS curves of different parts of C_{60} in Rec: the bottom (blue), the middle (red), and the top (black); the colors of PDOS curves match the colors of the atoms in the inserted C_{60}, the metal surface being horizontal and below in this view; the vertical green dashed lines around Fermi level enclose the most suitable energy range for the molecule to filter spin. (d) Spatial distribution of spin-down local DOS in the energy interval of [0, 0.2] eV (isovalue 0.0015 e/Bohr^3), viewed along the surface.

We plot the spin-polarized projected density of states (PDOS) of C_{60} for Rec and Unrec in Figure 2a, and the corresponding spin polarization ratio (SPR) in Figure 2b. The SPR is defined as $\mathrm{SPR}(E) = [\mathrm{DOS}_{\uparrow}(E) - \mathrm{DOS}_{\downarrow}(E)]/[\mathrm{DOS}_{\uparrow}(E) + \mathrm{DOS}_{\downarrow}(E)]$. Figure 2a shows that, compared to the free C_{60} monolayer, the interaction with Ni broadens the molecular orbitals due to the hybridization of C_{60} p orbitals and substrate d states.[9] These hybridizations enhance the PDOS of C_{60} near the Fermi level, changing the molecule from semiconducting to metallic. In particular, the PDOS of C_{60} at the Fermi level in Rec is 2.5 times that in Unrec. Therefore, we can expect a higher conductance in Rec than in Unrec. More importantly, due to the magnetic surface, the molecular DOS is spin polarized after adsorption, especially near the Fermi energy. According to the Julliere model of spin-dependent tunneling,[47] the MR of the system is positively correlated with the SPR at the Fermi energy. For an organic/ferromagnetic system, the PDOS at the interface is more relevant to a tunneling process than that in the bulk. From Figure 2b, the SPR in Rec is about 19% around the Fermi energy, almost three times that in Unrec, which is about 7%. Therefore, from the PDOS and SPR, we can expect that the surface reconstruction enhances the conductance and MR of C_{60} simultaneously. This feature meets the requirement of the miniaturization of read-head sensors, as we mentioned earlier.[3]

Another notable characteristic of Rec is the DOS distribution in C_{60}. We plot the average PDOS in the bottom, the middle, and the top parts of C_{60} (Figure 2c). It can be seen that these PDOS curves are quite different from each other. These differences mean that the delocalized molecular orbitals near the Fermi level in C_{60} are broken into groups of localized orbitals. We plot the local DOS in the energy interval of [0, 0.2] eV in Figure 2d to show the orbital distribution (the shape of the local DOS in [−0.2, 0] eV is similar). We can see that the states are localized at the equator of the C_{60}. In particular, from the middle PDOS in Figure 2c, we see that the PDOS at the C_{60} equator has a rather strong intensity near the Fermi level, and that the corresponding spin polarization at the Fermi level is significantly stronger than in the other two parts of the molecule. The PDOS at the equator has two advantageous features. One is that the Fermi level passes through the spin polarized peak, so these states can be accessed by a low bias voltage to reduce power dissipation. The other is that the polarized states are concentrated around the Fermi level so that a large current can be expected. Thus, the Rec system can hopefully be used as a basis of building highly efficient molecular spin filters that work in the bias window of ±0.2 eV, as is enclosed by green dashed lines in Figure 2c. This feature is not present in the Unrec structure.[27] The reason is as follows. In Unrec, only 0.6 electrons transfer into the three-fold degenerate lowest unoccupied molecular orbitals (LUMO) of C_{60}. Such a small electron transfer cannot significantly shift the C_{60} LUMO toward the Fermi level (Figure 2a). On the contrary, because of the reconstruction, 1.82 electrons transfer to C_{60}, and one LUMO orbital is supposed to be occupied. The partially occupied LUMO is the source of the states at the equator of C_{60}. The layer-dependent DOS character of C_{60} on Ni(111) is similar to that of a double-decker molecule after adsorption.[14] The difference is that here the reconstruction plays a key role.

In addition to the above changes in the molecule, the reconstruction also significantly modifies the magnetic structure of the surface. The calculated magnetic moments of the outermost nickel atoms in the Unrec and Rec cases are presented in Figure 1c,d. On the basis of the magnetic moment values and the internuclear distances from the molecule, the nickel atoms at the interface can be grouped into four types for both Rec and Unrec. For the unreconstructed case, four Ni atoms are strongly affected (atom types "i" and "j" in Figure 1c): these four, which are right beneath the molecule in the

DOI: 10.1021/jacs.5b10967
J. Am. Chem. Soc. 2016, 138, 4029−4035

outermost Ni layer, find their magnetic moments reduced to about 0.3 μ_B. Next to these four atoms, four other Ni atoms (type "k") are slightly influenced, converting their magnetic moments to 0.63 μ_B. Other atoms (type l") keep their clean surface value of 0.69 μ_B. By contrast, for the reconstructed case, all magnetic moments of the first Ni layer are significantly reduced. Six nickels (type "o") along the rim of the hole change their magnetic moments to 0.28 μ_B, while three others (type "p") change to about 0.44 μ_B. As the reconstruction removes seven top layer atoms, the C_{60} directly bonds to three nickels of the second layer (type "q") and consequently reduces their magnetic moments to 0.35 μ_B.

To further investigate the magnetic properties of the surface, we calculated the magnetic coupling and magnetocrystalline anisotropic energies (MAE) of the surface atoms. We used a Heisenberg model with a Hamiltonian $H = -\sum_{\alpha\neq\beta} J_{\alpha\beta}\boldsymbol{\mu}_\alpha\cdot\boldsymbol{\mu}_\beta$ to describe the first nearest neighbor magnetic interaction between Ni atoms and defined the magnetic coupling strength between atom α and atom β as $J_{\alpha\beta}\mu_\alpha\mu_\beta$; $J_{\alpha\beta}\mu_\alpha\mu_\beta$ was calculated from energy differences between properly selected couples of magnetic configurations.[48] For the clean unreconstructed surface, the coupling is 8.5 meV. From Table 1 we can see that the adsorption softens all the magnetic couplings between the surface atoms. This is similar to the finding of a previous study on Co interfaces.[18] The decreases of these magnetic coupling strengths are strongly correlated with the distance from the molecule and the bonding condition to the molecule.

Table 1. Magnetic Coupling Strengths $J_{\alpha\beta}\mu_\alpha\mu_\beta$ (in meV) between Different Types of Mutually Bonded Atoms at the Surface[a]

$\text{types}^{\text{Unrec}}$	$J_{\alpha\beta}\mu_\alpha\mu_\beta$	$\text{types}^{\text{Rec}}$	$J_{\alpha\beta}\mu_\alpha\mu_\beta$
ii	1.14	oo	2.16
ij	1.21	op	1.92
ik	2.51	or	2.22
il	2.39	pr	1.08
jk	2.62	qq	1.95
jl	2.94	qr	4.68
kl	7.21	rr	6.97
ll	7.00	-	-

[a]Here α, β = i, j, k, l for Unrec and α, β = o, p, q, r for Rec indicate different types of atoms as labeled in Figure 1c,d.

To analyze the reason for this softening, we examined the PDOS of the d orbitals of selected Ni atoms. These orbitals are grouped into d_π, which have out-of-surface-plane components ($d_\pi = d_{xz} + d_{yz} + d_{z^2}$), and d_σ which lies within the surface plane. A notable change is that the spin-down orbitals move to lower energy and the spin-up orbitals move in opposite direction so that the spin-split energy (E_{SS}) is reduced. We list the d-band-center shifts of the selected atoms relative to the clean unreconstructed surface and the corresponding decreases in E_{SS} in Table 2. We can see that the decreases of $E_{SS}^{d_\sigma} + E_{SS}^{d_\pi}$ on these atoms are qualitatively consistent with the reduction of the magnetic moments of the corresponding atoms, i.e., on the order of o ≈ i > q > p. Another feature is that the spin-down orbitals shift relatively more in the Ni atoms which have C−Ni bonds. Thus, the C−Ni bonds play an important role in the orbital shifts. As is demonstrated in valence bond theory,[49] 3d metals usually move some d electrons of majority spin into their minority orbitals and use the empty d orbitals to form new hybridized orbitals when forming bonds with organic compounds. So we conclude that the spin-down orbital shifts are caused by hybridization. Meanwhile, as the substrate loses electrons, the center of the total d orbitals must move to higher energy. Therefore, the spin-up orbitals move toward the Fermi level. These are the reasons for the relative energy shifts of d orbitals. The deformation of these PDOS are presented in Figure 3.

Table 2. Energy Shifts of d Band Centers Relative to the Clean Unreconstructed Surface and the Spin-Split Energy E_{SS} for Ni_o, Ni_p, Ni_q, and Ni_i (in eV) Defined in Figure 1[a]

types	d_σ^{up}	d_σ^{down}	$E_{SS}^{d_\sigma}$	d_π^{up}	d_π^{down}	$E_{SS}^{d_\pi}$
Ni_o	0.22	−0.19	0.27	0.14	−0.21	0.30
Ni_p	0.26	−0.01	0.41	0.21	−0.03	0.41
Ni_q	0.08	−0.20	0.40	−0.03	−0.36	0.32
Ni_i	0.09	−0.28	0.31	−0.01	−0.41	0.25
ref	0.00	0.00	0.68	0.00	0.00	0.65

[a]The reference d band centers are −1.49, −0.81, −1.39, and −0.74 eV for d_σ^{up}, d_σ^{down}, d_π^{up}, and d_π^{down}, respectively.

As is well-known, placing nonmagnetic atoms or molecules between magnetic atoms can induce a superexchange interaction between them. Estimating the magnitude of such interaction is helpful to understand the micromechanism behind the magnetic softening. A singe-site-mediated superexchange coupling can be evaluated by a fourth-order perturbation theory[50] to be $J_{\alpha\beta}\mu_\alpha\mu_\beta = \frac{t_{pd}^4}{\Delta_{pd}^2}\left(\frac{1}{\Delta_{pd}} + \frac{1}{U_{dd}}\right)$, where $t_{pd} = \langle ni|H|mj\rangle$ is the Hamiltonian matrix element between the nth orbital on the ith magnetic atom and the mth orbital on the jth mediating atom,[51] Δ_{pd} is the energy cost of a occupied p electron on a mediating atom moving into the lowest unoccupied d state on a magnetic atom, and U_{dd} is the smallest energy difference between the occupied and unoccupied d orbitals (Figure 3g). Because the electronic structure of the whole system is complicated and we only need a semiquantitative estimation of the antiferromagnetic part of the superexchange, we focus on the two selected cases as are shown in Figure 3f. In case 1, as the antiferromagnetic superexchange requires the angle of d−p −d to be about 180°, only the π_z orbital can serve as the media. We transform the Hamiltonian matrix into atomic basis sets and find that the $|t_{pd}|$ values range from 0.6 to 0.07 eV. Following prior methods,[52,53] we assign the energy level of p_z to be at −6.42 eV which is the location of the most intense peak in p_z PDOS. From the d orbital PDOS, the highest d occupied level is assigned to be at −0.56 eV and the lowest unoccupied d is assigned to be at 0.61 eV. The final result is weighted by the contributions of the corresponding peaks. According to our estimation, the total contribution of superexchange is 0.5 meV which is about 1 order of magnitude smaller than the reduction of the exchange coupling energy of 6.5 meV (Table 1). In case 2, we have a two-site-mediated process, and the superexchange couping can be evaluated as $\frac{t_{pd}^6}{\Delta_{pd}^4}\left(\frac{1}{\Delta_{pd}} + \frac{1}{U_{dd}}\right)$.[52] In this case, as the largest $|t_{pd}|$ is about 10% of Δ_{pd}, the contribution of such two sites mediated process should be of order 0.001 meV. Thus, the superexchange does not play a decisive role in the magnetic softening phenomenon in C_{60}/Ni(111), and the major reason is the change of DOS on Ni atoms.

The MAE are calculated from the difference of spin−orbit interaction (SOI) energies for spins along different axes. The

DOI: 10.1021/jacs.5b10967
J. Am. Chem. Soc. 2016, 138, 4029−4035

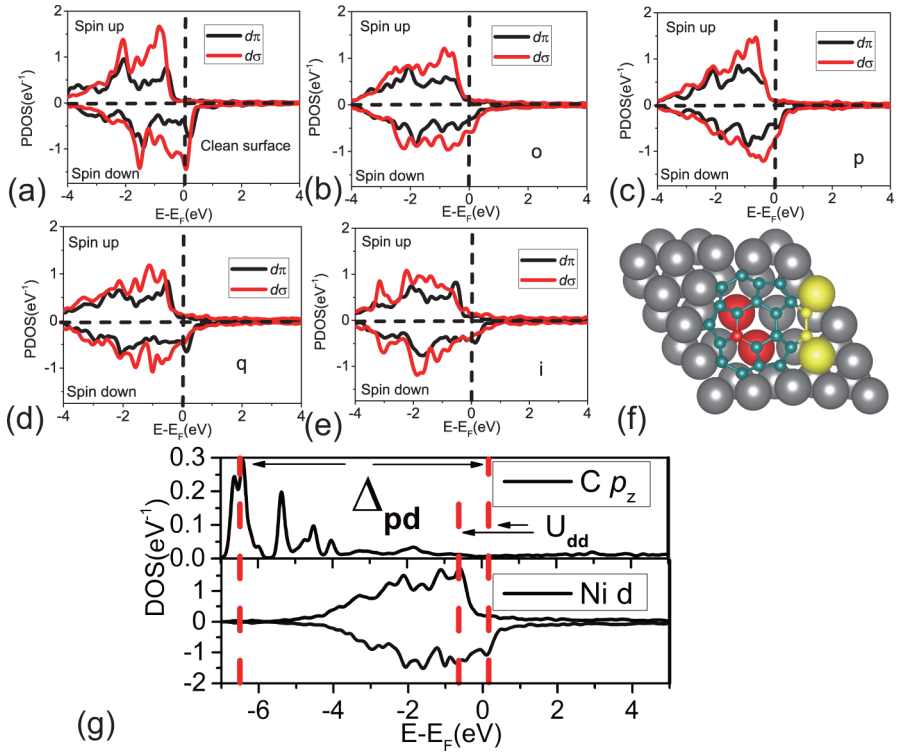

Figure 3. (a–e) PDOS of the Ni clean surface and selected Ni atoms with different environments; here the labels o, p, q, and i in (b–e) have the same meanings as in Figure 1; (f) selected atoms involved in superexchange processes: case 1 is colored red and case 2 yellow; (g) PDOS of Ni and C in case 1.

spin–orbit interaction can be calculated by noncollinear density functional theory (DFT) as well as a second-order perturbation for 3d transition metals $E_{SOI} = -\lambda^2 \sum_{u,o} \frac{|\langle o|\mathbf{L}\cdot\mathbf{S}|u\rangle|^2}{E_u - E_o}$,[54−56] where o and u denote occupied and unoccupied collinear Kohn–Sham orbitals and λ is a coupling constant. Note that our collinear Kohn–Sham orbitals have contained the information about surface symmetry breaking; thus, the Rashba and Dresselhaus terms have been included in this formula already. The MAE of each layer can be obtained by linking the results of these two methods. Values along the axes [111] (out of the surface plane), [101] and [112] (in plane, see Figure 1c) were obtained. The clean unreconstructed surface has an in-plane magnetization with a MAE of 0.24 meV/atom with degenerate energy for the easy axes [112] and [101].[57] After C_{60} adsorption, the MAE of the first layer becomes 0.14 and 0.03 meV/atom in Unrec and Rec, respectively. So we can conclude that the reconstruction has significant effect on MAE because it reduces 78% MAE of the outermost atom layer compared to the reconstructed case and 88% compared to the clean case. According to the classical explanation for the origin of MAE,[58] the vertical interaction reduces the stability of in-plane magnetization. Our result is consistent with this picture.

From the above results, we see that the adsorption of C_{60} on Ni(111) will soften the magnetism of the outermost Ni atoms. Such softening is significantly enhanced by reconstruction. Therefore, the reconstruction can be used as a convenient method to generate hard/soft composite magnetic structures to realize specific functions.[21]

CONCLUSIONS

In summary, we have theoretically determined the atomic structures of the C_{60}/Ni(111) surface system with and without reconstruction. The reconstruction not only stabilizes the molecule but also causes significant changes in the spintronic and magnetic properties at both sides of the organic/ferromagnetic interface. On the molecule side, by reconstruction, the DOS and SPR of the adsorbed molecule at the Fermi level are increased, which could simultaneously improve the conductance and MR of the system. The reconstruction also creates a new spin-polarized and energy-concentrated state at the equator of C_{60} near the Fermi energy, which makes it possible for the molecule to be used as a spin filter. This suggests that, instead of using double-decker molecules, one can also use three-dimensional molecules, such as fullerenes, to obtain layer-dependent spin-polarized states.[14] On the substrate side, reconstruction drastically reduces the exchange coupling and MAE of its outermost layer. The change of the exchange coupling can be related to the d-band shift under the influence of molecular adsorption. These findings reveal the importance of reconstruction on the organic/ferromagnetic interfaces, and could serve as basis for developing novel spintronic devices. Furthermore, in another investigation we found that C_{60} could induce a different type of reconstruction on the ferromagnetic Fe(100).[59] When we combine this result with the knowledge that C_{60} induces nonmagnetic metal surface reconstructions of different types, it is reasonable to believe that various reconstructions can also happen at other interfaces between different magnetic surfaces and molecules (e.g., C_{70}, thiolates, and graphene). Thus, our discoveries can be extended to other systems with various combinations between organic materials and magnetic surfaces.

DOI: 10.1021/jacs.5b10967
J. Am. Chem. Soc. 2016, 138, 4029–4035

■ ASSOCIATED CONTENT

Supporting Information

The Supporting Information is available free of charge on the ACS Publications website at DOI: 10.1021/jacs.5b10967.

Detail of structure determination, calculation method of MAE and vacancy formation energy, convergence tests of the slab model and atomic coordinates of the structures investigated (PDF)

■ AUTHOR INFORMATION

Corresponding Author

*shixq@sustc.edu.cn

Notes

The authors declare no competing financial interest.

■ ACKNOWLEDGMENTS

This work is supported in part by the National Natural Science Foundation of China (Grants 11474145 and 11334003). Michel A. Van Hove is supported by the HKBU Strategic Development Fund. We thank the National Supercomputing Center in Shenzhen for providing computation time, the High Performance Cluster Computing Centre, Hong Kong Baptist University, which receives funding from the Research Grants Council, University Grants Committee of the HKSAR and Hong Kong Baptist University, and National Supercomputing Center in Guangzhou, which receives funding from Special Program for Applied Research on Super Computation of the NSFC-Guangdong Joint Fund (the second phase).

■ REFERENCES

(1) Wood, R. *J. Magn. Magn. Mater.* **2009**, *321*, 555−561.
(2) Gao, K. Z.; Heinonen, O.; Chen, Y. *J. Magn. Magn. Mater.* **2009**, *321*, 495−507.
(3) Karpan, V. M.; Khomyakov, P. A.; Giovannetti, G.; Starikov, A. A.; Kelly, P. J. *Phys. Rev. B: Condens. Matter Mater. Phys.* **2011**, *84*, 153406.
(4) Boehme, C.; Lupton, J. M. *Nat. Nanotechnol.* **2013**, *8*, 612−615.
(5) Saraiva-Souza, A.; Smeu, M.; Zhang, L.; Souza, A. G.; Guo, H.; Ratner, M. A. *J. Am. Chem. Soc.* **2014**, *136*, 15065−15071.
(6) Yang, Z.; Zhang, B.; Liu, X.; Li, X.; Yang, Y.; Xiong, S.; Xu, B. *Phys. Chem. Chem. Phys.* **2014**, *16*, 1902−1908.
(7) Sanvito, S. *Chem. Soc. Rev.* **2011**, *40*, 3336−3355.
(8) Atodiresei, N.; Raman, K. V. *MRS Bull.* **2014**, *39*, 596−601.
(9) Galbiati, M.; Tatay, S.; Barraud, C.; Dediu, A. V.; Petroff, F.; Mattana, R.; Seneor, P. *MRS Bull.* **2014**, *39*, 602−607.
(10) Lazic, P.; Caciuc, V.; Atodiresei, N.; Callsen, M.; Bluegel, S. *J. Phys.: Condens. Matter* **2014**, *26*, 263001.
(11) Raman, K. V. *Appl. Phys. Rev.* **2014**, *1*, 031101.
(12) Atodiresei, N.; Brede, J.; Lazic, P.; Caciuc, V.; Hoffmann, G.; Wiesendanger, R.; Bluegel, S. *Phys. Rev. Lett.* **2010**, *105*, 066601.
(13) Atodiresei, N.; Caciuc, V.; Lazic, P.; Bluegel, S. *Phys. Rev. B: Condens. Matter Mater. Phys.* **2011**, *84*, 172402.
(14) Callsen, M.; Caciuc, V.; Kiselev, N.; Atodiresei, N.; Bluegel, S. *Phys. Rev. Lett.* **2013**, *111*, 106805.
(15) Rocha, A. R. *Physics* **2013**, *6*, 96.
(16) Schwoebel, J.; Fu, Y.; Brede, J.; Dilullo, A.; Hoffmann, G.; Klyatskaya, S.; Ruben, M.; Wiesendanger, R. *Nat. Commun.* **2012**, *3*, 953.
(17) Brede, J.; Atodiresei, N.; Caciuc, V.; Bazarnik, M.; Al-Zubi, A.; Bluegel, S.; Wiesendanger, R. *Nat. Nanotechnol.* **2014**, *9*, 1018−1023.
(18) Raman, K. V.; Kamerbeek, A. M.; Mukherjee, A.; Atodiresei, N.; Sen, T. K.; Lazic, P.; Caciuc, V.; Michel, R.; Stalke, D.; Mandal, S. K.; Bluegel, S.; Muenzenberg, M.; Moodera, J. S. *Nature* **2013**, *493*, 509−513.
(19) Decker, R.; Brede, J.; Atodiresei, N.; Caciuc, V.; Bluegel, S.; Wiesendanger, R. *Phys. Rev. B: Condens. Matter Mater. Phys.* **2013**, *87*, 041403.
(20) Bairagi, K.; Bellec, A.; Repain, V.; Chacon, C.; Girard, Y.; Garreau, Y.; Lagoute, J.; Rousset, S.; Breitwieser, R.; Hu, Y. C.; Chao, Y. C.; Pai, W. W.; Li, D.; Smogunov, A.; Barreteau, C. *Phys. Rev. Lett.* **2015**, *114*, 247203.
(21) Lopez-Ortega, A.; Estrader, M.; Salazar-Alvarez, G.; Roca, A. G.; Nogus, J. *Phys. Rep.* **2015**, *553*, 1−32.
(22) Guldi, D. M.; Illescas, B. M.; Atienza, C. M.; Wielopolskia, M.; Martin, N. *Chem. Soc. Rev.* **2009**, *38*, 1587−1597.
(23) Gobbi, M.; Golmar, F.; Llopis, R.; Casanova, F.; Hueso, L. E. *Adv. Mater.* **2011**, *23*, 1609−1613.
(24) Tran, T.; Le, T. Q.; Sanderink, J. G.; van der Wiel, W. G.; de Jong, M. P. *Adv. Funct. Mater.* **2012**, *22*, 1180−1189.
(25) Zhang, X.; Mizukami, S.; Kubota, T.; Ma, Q.; Oogane, M.; Naganuma, H.; Ando, Y.; Miyazaki, T. *Nat. Commun.* **2013**, *4*, 1392.
(26) Zhang, X.; Mizukami, S.; Ma, Q.; Kubota, T.; Oogane, M.; Naganuma, H.; Ando, Y.; Miyazaki, T. *J. Appl. Phys.* **2014**, *115*, 172608.
(27) Yoshida, K.; Hamada, I.; Sakata, S.; Umeno, A.; Tsukada, M.; Hirakawa, K. *Nano Lett.* **2013**, *13*, 481−485.
(28) Stengel, M.; Vita, A. D.; Baldereschi, A. *Phys. Rev. Lett.* **2003**, *91*, 166101.
(29) Pai, W. W.; Hsu, C. L.; Lin, M. C.; Lin, K. C.; Tang, T. B. *Phys. Rev. B: Condens. Matter Mater. Phys.* **2004**, *69*, 125405.
(30) Tang, L.; Zhang, X.; Guo, Q.; Wu, Y.-N.; Wang, L.-L.; Cheng, H.-P. *Phys. Rev. B: Condens. Matter Mater. Phys.* **2010**, *82*, 125414.
(31) Shi, X.-Q.; Van Hove, M. A.; Zhang, R.-Q. *J. Mater. Sci.* **2012**, *47*, 7341−7355.
(32) Shi, X.; Pang, A.; Man, K.; Zhang, R.; Minot, C.; Altman, M.; Van Hove, M. A. *Phys. Rev. B: Condens. Matter Mater. Phys.* **2011**, *84*, 235406.
(33) Shi, X.-Q.; Van Hove, M. A.; Zhang, R.-Q. *Phys. Rev. B: Condens. Matter Mater. Phys.* **2012**, *85*, 075421.
(34) Forster-Tonigold, K.; Gross, A. *Surf. Sci.* **2015**, *640*, 18−24.
(35) Maksymovych, P.; Sorescu, D. C.; Voznyy, O.; Yates, J.; John, T. *J. Am. Chem. Soc.* **2013**, *135*, 4922−4925.
(36) Hsu, B. C.; Lin, C.-Y.; Hsieh, Y.-S.; Chen, Y.-C. *Appl. Phys. Lett.* **2012**, *101*, 243103−243103−4.
(37) Kiguchi, M.; Iizumi, K.-i.; Saiki, K.; Koma, A. *Appl. Surf. Sci.* **2003**, *212*, 101−104.
(38) Kusch, C.; Winter, B.; Mitzner, R.; Silva, A. G.; Campbell, E.; Hertel, I. *Chem. Phys. Lett.* **1997**, *275*, 469−476.
(39) Lin, C. H.; Lin, K. C.; Tang, T. B.; Pai, W. W. *J. Nanosci. Nanotechnol.* **2008**, *8*, 602−607.
(40) Kresse, G.; Furthmller, J. *Comput. Mater. Sci.* **1996**, *6*, 15−50.
(41) Kresse, G.; Joubert, D. *Phys. Rev. B: Condens. Matter Mater. Phys.* **1999**, *59*, 1758.
(42) Perdew, J. P.; Burke, K.; Ernzerhof, M. *Phys. Rev. Lett.* **1996**, *77*, 3865.
(43) Giannozzi, P.; Baroni, S.; Bonini, N.; Calandra, M.; Car, R.; Cavazzoni, C.; Ceresoli, D.; Chiarotti, G. L.; Cococcioni, M.; Dabo, I. *J. Phys.: Condens. Matter* **2009**, *21*, 395502.
(44) Shi, X.-Q.; Van Hove, M. A.; Zhang, R.-Q. *Phys. Rev. B: Condens. Matter Mater. Phys.* **2012**, *85*, 075421.
(45) Pai, W. W.; Jeng, H.; Cheng, C.-M.; Lin, C.-H.; Xiao, X.; Zhao, A.; Zhang, X.; Xu, G.; Shi, X.; Van Hove, M. *Phys. Rev. Lett.* **2010**, *104*, 036103.
(46) Tang, W.; Sanville, E.; Henkelman, G. *J. Phys.: Condens. Matter* **2009**, *21*, 084204.
(47) Julliere, M. *Phys. Lett. A* **1975**, *54*, 225−226.
(48) Xiang, H.; Lee, C.; Koo, H.-J.; Gong, X.; Whangbo, M.-H. *Dalton Trans.* **2013**, *42*, 823−853.
(49) Lawrance, G. A. *Introduction to Coordination Chemistry*; John Wiley and Sons: West Sussex, U.K., 2013.
(50) Jefferson, J. H. *J. Phys. C: Solid State Phys.* **1988**, *21*, L193−L197.
(51) Gunnarsson, O. *Alkali-Doped Fullerides: Narrow-Band Solids with Unusual Properties*; World Scientific: Singapore, 2004.

DOI: 10.1021/jacs.5b10967
J. Am. Chem. Soc. 2016, 138, 4029−4035

(52) Toyoda, M.; Saito, T.; Yamauchi, K.; Shimakawa, Y.; Oguchi, T. *Phys. Rev. B: Condens. Matter Mater. Phys.* **2015**, *92*, 014420.
(53) Mori, T.; Katsuhara, M. *J. Phys. Soc. Jpn.* **2002**, *71*, 826−844.
(54) Bhandary, S.; Ghosh, S.; Herper, H.; Wende, H.; Eriksson, O.; Sanyal, B. *Phys. Rev. Lett.* **2011**, *107*, 257202.
(55) Wang, D.-s.; Wu, R.; Freeman, A. *Phys. Rev. B: Condens. Matter Mater. Phys.* **1993**, *47*, 14932.
(56) Kota, Y.; Sakuma, A. *J. Phys. Soc. Jpn.* **2014**, *83*, 034715.
(57) Bruno, P. Physical origins and theoretical models of magnetic anisotropy In *Physical Origins and Theoretical Models of Magnetic Anisotropy*; Dederichs, P., Grnberg, P., Zinn, P., Eds.; Forschungszentrum Julich: Julich, 1993; Chapter 24, pp 24.1−24.28.
(58) Stohr, J.; Siegmann, H. *Magnetism: From Fundamentals to Nanoscale Dynamics*; Springer: Berlin, 2007.
(59) Yang, Z.-H.; Pang, R.; Shi, X.-Q. *J. Phys. Chem. C* **2015**, *119*, 10532.

DOI: 10.1021/jacs.5b10967
J. Am. Chem. Soc. 2016, 138, 4029−4035